

Article

Contamination- and Perturbation-Free Fluorescent Monitoring of Zn²⁺ in Suspensions Using Crown Ether-Functionalized Magnetic Nanoparticles

Panna Vezse¹, Ádám Golcs^{1,2,*} , Tünde Tóth^{1,3} and Péter Huszthy^{1,*} 

¹ Department of Organic Chemistry and Technology, Budapest University of Technology and Economics, Szent Gellért tér 4, H-1111 Budapest, Hungary; panna.vezse@edu.bme.hu (P.V.); toth.tunde@vbk.bme.hu (T.T.)

² Department of Pharmaceutical Chemistry, Semmelweis University, Hőgyes Endre utca 9, H-1092 Budapest, Hungary

³ Centre for Energy Research, Konkoly-Thege Miklós út 29-33, H-1121 Budapest, Hungary

* Correspondence: golcs.adam@edu.bme.hu (Á.G.); huszthy.peter@vbk.bme.hu (P.H.)

Abstract: This study aims to introduce a fluorescence-based chemosensing method for Zn²⁺ in aqueous suspensions and untreated surface waters, conditions which generally hinder the application of conventional optochemical sensing platforms. A macrocyclic fluoroionophore was covalently bonded to a silica-coated magnetic nanoparticle and applied according to a predetermined protocol for analyzing trace amounts of Zn²⁺ under rarely investigated conditions. Utilizing the reversible complexation of the immobilized fluoroionophore, rapid regeneration was carried out via simple acidification after the magnetic-assisted solid-phase extraction of the particles. Forming inclusion complexes with Zn²⁺ with the receptor units of the particles leads to a significant enhancement in fluorescence intensity at 370 nm, above the detection limit of 5 ppb, with a dynamic linear range of quantification of 15–3000 ppb in a pH range of 5.5–7.5. Practical applicability was confirmed by analyzing untreated river water and an aqueous suspension of pumpkin seed flour as real and relevant heterogeneous multicomponent samples of predetermined sample composition and natural Zn²⁺ content. Our practical approach aims to broaden the applicability range of optochemical sensing platforms for Zn²⁺.

Keywords: magnetic nanoparticle; fluorescence; zinc; molecular recognition



Citation: Vezse, P.; Golcs, Á.; Tóth, T.; Huszthy, P. Contamination- and Perturbation-Free Fluorescent Monitoring of Zn²⁺ in Suspensions Using Crown Ether-Functionalized Magnetic Nanoparticles. *Chemosensors* **2023**, *11*, 547. <https://doi.org/10.3390/chemosensors11100547>

Academic Editors: Marko Spasenovic, Guo-Hui Pan and Young-Tae Chang

Received: 27 August 2023
Revised: 12 October 2023
Accepted: 20 October 2023
Published: 22 October 2023



Copyright: © 2023 by the authors. Licensee MDPI, Basel, Switzerland. This article is an open access article distributed under the terms and conditions of the Creative Commons Attribution (CC BY) license (<https://creativecommons.org/licenses/by/4.0/>).

1. Introduction

The contamination of samples with sensor molecules or the presence of perturbation-causing physical contaminants (precipitates, insoluble particles in suspensions, colloids, etc.) can hold back the potential of optochemical sensing among analytical techniques. Sensor molecules are usually immobilized to solid carriers to overcome these limitations [1–3]. One favorable option is anchoring them to magnetic nanoparticles (MNPs), which also provides a simple magnetic facilitated recovery [4]. Following these considerations, we decided to covalently attach a Zn²⁺-selective fluorescent macrocycle to the surface of a silica-coated MNP to gain a multiple-use chemosensing platform for Zn²⁺. We intended to focus especially on suspensions and untreated surface water samples, as their investigation is considered as the bottleneck of ion-selective optochemical analysis by using conventional optode devices (i.e., membrane, optical fiber, flow-through, film and waveguide optodes). In the cases of the mentioned types of optodes, the presence of physical contaminants—i.e., large particles, sand, slurry, macromolecular contaminants, etc.—can hinder applicability, as these contaminants tend to cover the active signaling sites, thus partially blocking the way of light on the source or detector side.

Zn²⁺ plays a crucial role in biology [5]; thus, many selective applications have been developed for its determination in various samples [6,7]. However, most of them lack

appropriate selectivity, especially in distinguishing Cd^{2+} and Zn^{2+} , owing to their quite similar properties and usual copresence in nature [8]. Compared to the most commonly investigated slightly contaminated aqueous samples, optical chemosensing in heterogeneous solid–liquid systems, like real soil samples or suspensions, is more challenging, and would present great potential [8]. Although the typical concentration of Zn^{2+} in groundwater is around 0.04 ppm, the concentration in drinking water is usually higher due to plumbing networks [9]. From the aspect of sensor development, the limit of detection (LOD) of the new applications should meet the permissible Zn^{2+} concentration in drinking water, which is currently 5 ppm [9]. The rising industrial activities inevitably cause an increased Zn^{2+} content in rivers and soils, which can reach 20 and 500 ppm, respectively [10,11].

The benefits of combining the advantageous selectivity of supramolecular interactions and the specific surface properties of nanomaterials are well-known and lead to the development of numerous useful tools, both for academia and industry [12–17]. Combining nanostructural carriers and molecular cages simultaneously provides the regenerability, separability, high surface area, adsorption capacity, etc. [12–17]. Crown ethers are among the oldest synthetic receptors. Despite their less advanced selectivity compared to that of 21st-century sensor molecule alternatives, they are still widely used due to their structural simplicity and better availability. They have also been used for several decades in ion-selective optochemical sensing. In the case of the first generation of optodes, crown ethers had the role of selectoionophores, while optical signals were induced via the indirect protonation process of a chromoionophore at the same time [18]. As the proposed sensor molecule contains the fluorophore as a subunit of its coordination sphere, it can perform both molecular recognition and direct-type optical signaling. The advantage of using the ion-selective macrocycles instead of the most commonly applied introduction of simple functional groups in the particle surface is their improved selectivity. It is attributed not only to the lack of size-, shape- and polarity-specific molecular cages, but also to the occurrence of only charge-driven intermolecular interactions with simple functionalized surfaces. Polar functional groups on the particle surface, especially negatively charged ones (i.e., $-\text{COO}^-$, $-\text{S}^-$), can coordinate not only competing cations with the same chemical character and charge, but unfortunately, they also provide unspecific binding sites for various contaminants in the samples (organic content, physical contaminants containing biomolecules, natural surfactants, etc.) in contrast to neutral crown ethers as stereoelectronic host molecules with a multipoint binding ability. However, it is also true that macrocycle-functionalized nanoparticles are naturally more expensive due to the need for preparing receptor units and their difficult subsequent immobilization on the surface, while the introducible number of binding sites would be far behind that provided by simple surface functional groups.

Surface functionalization plays a critical role in this type of application, as the chemical properties as well as the number of ligands and functional groups on the surface of the NPs largely influence their charge, dispersibility, and colloidal stability, as well as the hydrophilicity/hydrophobicity, processability, and interactions with the medium [19]. Furthermore, suitable functional groups or coatings on NPs enable the controlled functionalization via covalent binding of functional molecules, such as crown ethers, as synthetic receptors capable of providing molecular recognition. We used a commercially available silica-coated MNP as a prefunctionalized core of the sensing unit. For further modification, we applied an upgraded specific version of a reported method, which was successfully used previously in our research group for functionalizing silica gel surfaces with crown ethers [20]. In the context of the present work, we also proved that this method is suitable for the surface modification of silica-coated MNPs—not only for spherical silica gels—by providing a molecular linker of a proper length (3 C–C-bond-length) for preserving optimal complexing properties. It was also important to consider that the applied functionalized NPs needed to show proper colloidal stability in water, even after post-coating modifications, besides providing the unchanged complexation of the receptor. To preserve the relatively sensitive sensor molecule in its original form, mild reaction conditions should

be applied for the chemical modification of the MNP surface. Furthermore, allowing for bioanalytical applicability and the minimization of unspecific adsorption sites without any further surface passivation strategies—which might cause the inactivity of the receptor—were also required [19,21]. This means avoiding the introduction of a large number of highly polar, especially negatively charged, functional groups, which can coordinate several cations without a predetermined selectivity. The proposed silica-coated core was previously applied many times while satisfying the former essential requirements [22–27].

Due to the enhanced importance of rapid chemosensing and the inherent advantages of fluorescent detection, recent research shows tremendous growth in the number of published papers focusing on the fluorescent detection of Zn^{2+} [28,29]. Among them, the following can be highlighted in the context of the present paper:

Kim et al. reported a naphthylamide- and Fe_3O_4 -containing NP for the selective detection of Zn^{2+} [8]. The NP had a naphthalimide and a dipicrylamine moiety as the Zn^{2+} -coordinating subunit and catechol-linked Fe_3O_4 as the magnetic core. A weak fluorescence was obtained at 527 nm upon excitation at 370 nm in DMSO-HEPES buffer, while the presence of Zn^{2+} induced the fluorescence enhancement. The NP was exploited for the detection and removal of Zn^{2+} from soil samples [8].

Li et al. reported a new fluorescent and surface-enhanced Raman spectroscopic dual-mode Zn^{2+} probe based on a modified gold NP [30]. Since Zn^{2+} caused the self-aggregation of the particles and a parallel fluorescence enhancement at 425 nm, it enabled a selective chemosensing application, even the detection of the distribution of Zn^{2+} in single cells, with an excellent biocompatibility and low cytotoxicity [30].

A BODIPY-based Zn^{2+} -selective fluorescence sensor was developed by Jia et al. [31]. The *N,N*-di(pyridin-2-ylmethyl)-ethane-1,2-diamine group provided a binding site for Zn^{2+} . In the absence of Zn^{2+} , fluorescent monomers self-assembled to form NPs, which resulted in a quenched fluorescence via aggregation. In the presence of Zn^{2+} , it coordinated to the aggregates, resulting in a returned fluorescence at 600 nm (while excited at 573 nm) [31].

Wu et al. reported a fluorescent Ag_2S quantum dot, which emitted at 1100 nm (excitation at 480 nm) [32]. In this case, the Ag_2S nanocrystals with *n*-dodecylmercaptan-linked thioglycolic acid functions could act as monodisperse spherical NPs in water, turning on a fluorescent response for Zn^{2+} . Upon the addition of Zn^{2+} , it binds to the thioglycolic acids on the particle surface, thereby forming a Zn-mercapto-derivative as a complex passivation shell on the surface of the Ag_2S quantum dots. This process restores surface defects, inhibits the non-radiation recombination pathway, and enhances the intensity of fluorescence emission at 1100 nm, thus making the probe able to be used in the NIR-II fluorescence detection of Zn^{2+} [32].

Pourfallah et al. reported the first 4-aminoquinoline-based reusable nanochemosensor for Zn^{2+} [33] with PEG-linked $Fe_3O_4@SiO_2$ -PEG-4AQ and $Fe_3O_4@SiO_2$ -4AQ magnetic cores. Red shift and a 13.5-fold fluorescent enhancement were observed upon complexation with Zn^{2+} , with a detection limit of 0.0065 $\mu\text{mol/L}$, showing a reversible operation upon treatment with EDTA [33].

A fluorometric assay for Zn^{2+} was reported by Shen et al., which relies on the use of an isothermal cycle to amplify the fluorescence signal, and of magnetic beads to completely remove unreacted DNA detection probes [34]. The sensor had a detection limit as low as 33 fmol/L, and was successfully applied for the determination of Zn^{2+} in spiked tap water and seawater samples, as well as in infant milk powder and breast milk [34].

Continuing these recent efforts, we aimed to create the first crown ether-functionalized MNP for the fluorescent determination of Zn^{2+} . Herein, we present a method which allows for a uniquely simple regeneration, using only extraction with slightly acidic water, and also a very high selectivity due to the inclusion-type complexation of the applied fluoroionophore. Furthermore, the introduced measurement protocol enables the component selective analysis of suspensions, which can rarely be performed using other optochemical sensors. Moreover, an analysis of real samples was performed without any preliminary sample preparation (filtration, preconcentration/dilution, pH adjustment, etc.).

2. Experimental

2.1. Materials and Instruments

The chemicals were purchased from Sigma-Aldrich Corporation (St. Louis, MO, USA, owned by Merck, Darmstadt, Germany) and were used without further purification unless otherwise noted. A commercially available silica-coated MNP, TurboBeads™ Silica, was used as a magnetic nanocore for further functionalization. It has a carbon content of ≤ 14 wt%, a cobalt magnetic core, a magnetism of ≥ 100 emu/g mass saturation, a 20–40 nm average diameter, a specific surface area of ≥ 15 m²/g, and high stability in the air (weight gain in the air at 100 °C < 3 wt%).

An acridino-diaza-20-crown-6 ether containing reactive allyl groups (**1**, see Figure 1) was used as a direct-type fluorescent sensor molecule [35]. Covalent attachment to the silica-coated surface of the MNP was performed through the reaction of the allyl units via a 3-C-atom-containing molecular spacer.

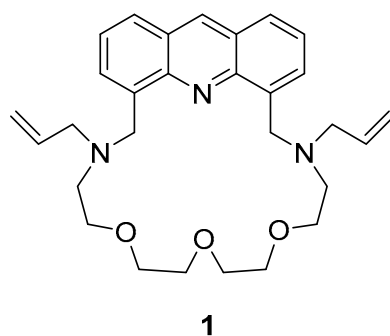


Figure 1. The applied Zn²⁺-selective fluorescent sensor molecule (**1**).

This fluoroionophore can fulfill receptor and signaling functions simultaneously. Its selectivity was previously proved in a solution phase [35]. The ionophore preferred Zn²⁺ ($\log K = 5.6$, $\Delta \log K > 4.0$ in each case) over 20 other potential competing cations (Rb²⁺, Li⁺, Cs⁺, Mn²⁺, Fe²⁺, Ba²⁺, Sr²⁺, Hg²⁺, Cd²⁺, K⁺, Ni²⁺, Co²⁺, Na⁺, Cu²⁺, Ag⁺, Ca²⁺, Mg²⁺, Cr³⁺, Pd²⁺, Pb²⁺) and showed a reversible complex formation with a 1:1 stoichiometry. Only Al³⁺ and Bi³⁺ interfered, but these ions are rarely present as contaminants in practice. The coordination of anions (H₂PO₄⁻, NO₃⁻, HSO₄⁻, CH₃COO⁻, F⁻, Cl⁻, Br⁻, I⁻) is also not expected, even when the ionophore is protonated [35].

UV/Vis spectra were recorded on a UNICAM UV4-100 spectrophotometer, controlled using the VIZION 3.4 software (ATI UNICAM, UK). Fluorescence emission spectra were recorded on a Perkin-Elmer LS 50B luminescent spectrometer (PerkinElmer Inc., Waltham, MA, USA) and were corrected using the FL Winlab 3.0 spectrometer software (PerkinElmer Inc., Waltham, MA, USA). Quartz cuvettes with a path length of 1 cm were used in all cases. Zn²⁺-acetate was used for preparing all artificial samples. Spectroscopic measurements were carried out at room temperature (25 ± 1 °C). During the spectrophotometric titrations, the solutions were added with a Hamilton-syringe to the aqueous solutions in the spectrophotometric cuvette. The results were corrected with the background signal and the dilution effect of the added solutions. OriginPro 8.6 (OriginLab Corp., Northampton, MA, USA) software was used for the evaluation and visualization of the spectroscopic results. Every reported point comes from at least three independent measurements.

For the pH measurements, a Mettler Toledo SevenEasy pH meter (Mettler Toledo, Columbus, OH, USA), fitted with a Mettler Toledo Inlab microelectrode, was used. The various pH values were adjusted with nitric acid and an aqueous sodium hydroxide solution. The accuracy of the pH determinations was within ±0.1 unit.

In the cases of multielement sample compositions, like real samples, the element masses were determined via inductively coupled plasma optical emission spectroscopy (ICP-OES). Sample solutions of 5 mL were acidified with 50 µL of nitric acid (63 wt%). The sample solutions were measured in simultaneous, multielement mode using a Labtest

Plasmalab ICP-spectrometer (Labtest Equipment Company, Valparaiso, IN, USA) with a 40-channel Paschen–Runge vacuum polychromator with photomultiplier detectors. Additional information on the instrumentation and measurement settings can be found in the Supplementary Materials.

In the case of selectivity studies, 23 different metal salts were used: carbonate counterion: Rb^{2+} , Li^+ , Cs^+ ; sulfate counterion: Mn^{2+} , Fe^{2+} ; hydroxide counterion: Ba^{2+} ; chloride counterion: Sr^{2+} , Al^{3+} , Hg^{2+} , Bi^{3+} ; iodide counterion: Cd^{2+} ; acetate counterion: K^+ , Ni^{2+} , Co^{2+} , Na^+ , Cu^{2+} , Ag^+ , Ca^{2+} , Zn^{2+} , Mg^{2+} ; nitrate counterion: Cr^{3+} , Pd^{2+} , Pb^{2+} . These were added separately to the aqueous colloid dispersion of the fluorescent MNP in the form of 50 mM aqueous solutions.

Validation was carried out by measuring untreated (containing floating physical contaminants, e.g., sand, etc.) river water from the Danube and aqueous suspensions of pumpkin seed flour. Detailed information regarding the composition of both the river water and the flour can be found in the Supplementary Materials.

2.2. Determination of Limit of Detection and Quantitation and Response Time

The detection limits (LOD) and limit of quantitation (LOQ) were calculated by using the data of the fluorescence titrations. To determine the signal-to-noise ratio, the fluorescence intensity of the MNP was measured nine times, and the standard deviation of these blank measurements was determined. Three separate measurements of the emission intensity were performed in the presence of Zn^{2+} , and the average of the intensities was plotted as a function of the Zn^{2+} concentration to determine the slope of the linear regression (see Supplementary Materials). The LOD and LOQ were calculated based on a standard method [36], as follows:

$$\text{LOD} = \frac{3d}{S} \quad (1)$$

$$\text{LOQ} = \frac{10d}{S} \quad (2)$$

where d is the standard deviation of the optical signal of the sensor membrane and S is the slope of linear regression for the emission intensities as a function of the concentration of Zn^{2+} .

The response time was defined as the time required to reach 95% of a constant optical response.

3. Results and Discussion

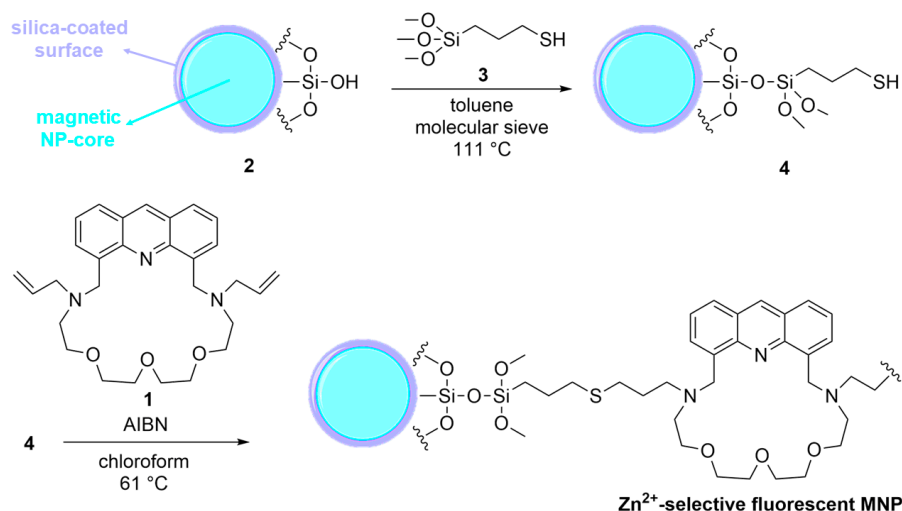
3.1. Surface Modification of Silica-Coated Magnetic Nanoparticles

The modification of the silica-coated surface-layer of the MNP (2) was carried out based on a previously reported two-step procedure for modifying spherical silica gels [20]. Some changes were introduced to modify this reported method for MNPs.

A slurry of the silica-coated MNP (2, 150 mg) in dry toluene (1.5 mL) was heated with magnetic stirring (using an external magnetic stirrer by exploiting only the magnetic properties of the NP) to reflux under argon for 12 h. The formed water was removed by adding a 3 Å molecular sieve (300 mg). After adding (γ -mercaptopropyl)-trimethoxysilane (3, 300 μL , 1.53 mmol), the mixture was stirred in the above conditions for 48 h. The mixture was cooled down to 25 °C the modified MNP (4) was collected by using an external magnet and then washed sequentially with toluene (5.0 mL), CHCl_3 (5.0 mL), MeOH (5.0 mL), and CHCl_3 (5.0 mL).

As a second step, the modified MNPs containing the reactive linkers (4) were directly transferred to the reaction with crown ether (1) in the form of a slurry in CHCl_3 (evaporation to dryness should not be applied to avoid the aggregation of the MNPs). The slurry of the linker-functionalized MNP (4, 1.0 mL), macrocyclic fluoroionophore (1, 30 mg, 0.06 mmol) and 2,2'-azobis(2-methyl)propionitrile (AIBN, 3.0 mg, 0.02 mmol) in freshly distilled pure and dry CHCl_3 (2.0 mL), was heated with magnetic stirring at 50 °C under argon for

48 h; two additional portions of AIBN (3.0 mg, 0.02 mmol each) were added after 12 and 24 h. After cooling to 25 °C, the fluorescent MNPs were collected with a permanent external magnet and washed sequentially with CHCl₃ (5.0 mL), MeOH (5.0 mL), and H₂O (3 × 5.0 mL). The synthetic steps of the functionalization are shown in Scheme 1.



Scheme 1. Procedure for the functionalization of silica-coated MNPs (2).

The modification procedure caused a partial aggregation of the MNPs (probably due to mechanical stirring and/or the bifunctional nature of the sensor molecule); thus, larger ones formed in the suspension. These aggregates were separated via sedimentation to gain a stable colloidal dispersion in water. The particles were added in the form of these aqueous colloidal dispersions to the samples for fluorescence studies. All of the measurements were performed within 24 h, while the colloidal dispersion of the functionalized MNPs remained stable.

Neither combustion analysis nor FTIR measurements could be used for determining the loading density of macrocycle 1, since the portion of them on the surface did not prove to be enough for achieving a proper determination. That is why UV/Vis titration was carried out to obtain a calibration curve for the fluoroionophore (1), and the portion of the attached amount of the sensor molecule (1) was calculated according to the Lambert–Beer equation (detailed information can be found in the Supplementary Materials). The results show that the functionalized MNPs contain ~3.3 wt% covalently immobilized sensor molecules on their surfaces. The presence of some non-fluorescent particles cannot be excluded; they, just like inactive ionophores, reduce sensitivity by causing background signals. However, the probability for particles to remain non-fluorescent is very small. A rough estimation for the average number of immobilized crown ethers resulted in a number of about 10¹⁴ pieces of molecules per nanoparticles. Five parallel measurements were carried out after proving the effectiveness of removing the remaining unbonded sensor molecules. Centrifugation and a subsequent spectrophotometrical investigation of the filtrate were used for checking the presence of the physically (not covalently) adsorbed fluoroionophores.

3.2. Measurement Procedure

The Zn²⁺ content of samples in solution, or even in suspension, can be measured by directly adding a water-based colloid dispersion of the functionalized MNPs (Step 1 in Figure 2). The optimal ratio is as follows: 1.0 mg of MNPs in 1.0 mL of distilled water to 4.0 mL of sample (optimized for the linear working range of the probe, see Section 3.3). Then, the samples need to be mechanically stirred to reach a homogeneous distribution of dissolved Zn²⁺ in the medium (Step 2 in Figure 2). After stirring, some incubation time is required to let the suspension sediment fall to the bottom of the vial. Following sedimentation, the MNPs can be easily separated by using a permanent magnet externally

(Step 3 in Figure 2); thus, the sediment and suspension phase of the sample can be removed via pipetting. (In the case of homogeneous samples, analysis can be directly performed without sedimentation.) During this process, a part of the sensor molecules form inclusion complexes with the dissolved Zn^{2+} on the surface of the physically segregated MNPs. This is followed by diluting the segregated MNP slurry to the volume corresponding to the initial state (Step 4 in Figure 2). Finally, the content of the vial is shaken well to gain a homogeneously distributed colloid again, and the latter, containing the macrocycle 1- Zn^{2+} complexes, is analyzed using a conventional fluorescent spectrophotometer to determine the Zn^{2+} content based on the spectral changes (Steps 5–6 in Figure 2).

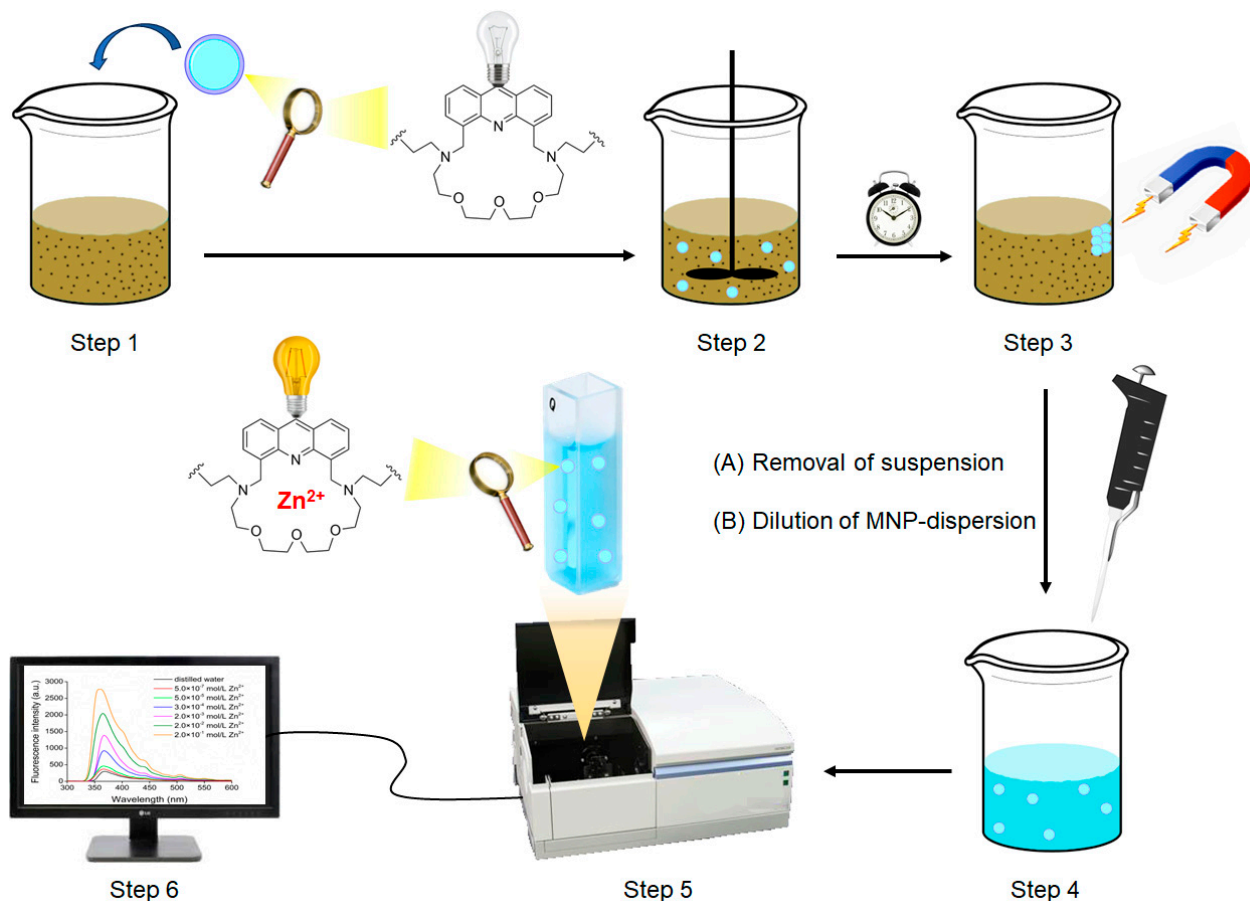


Figure 2. The applied measurement protocol for sample analysis.

It is clear from the applied protocol that it only enables the determination of the dissolved Zn^{2+} inside the heterogeneous samples. If there is a need to study the content of the solid part of the samples, additional treatments of the samples (e.g., using strong acid) have to be initially performed.

After the determination of Zn^{2+} , the applied MNPs can be used several more times. The regeneration, i.e., the removal of the complexed Zn^{2+} from the macrocycle cavity, can be performed by using a slightly acidic (pH = 4.0 aqueous solution of nitric acid) extraction. The dispersion should be diluted and shaken two times with an equivalent volume of the acidic solution while separating the MNPs. The third extraction should be carried out with an aqueous pH = 9.0 sodium hydroxide solution to convert fluoroionophore 1 back to its neutral form. The mechanism of the facilitated decomplexation can be seen in Figure 3.

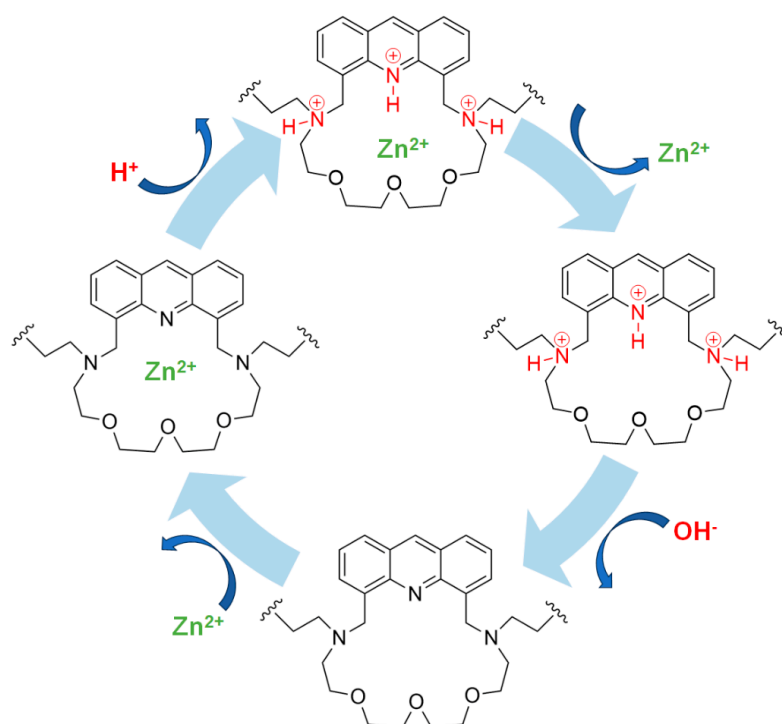


Figure 3. Acid-induced decomplexation of the immobilized sensor molecule (1) on the surface of the MNP during the regeneration cycle.

It is advantageous that no chelating additives (i.e., EDTA) are needed compared to many other methods. The slightly acidic medium first causes the protonation of the basic tertiary-*N*-atoms and then also the weakly basic acridine-*N* of the macrocycle (1), which results in the loss of their electron donor ability, leading to the dissociation of the complexed Zn^{2+} from the molecular cage.

3.3. Fluorescence Response to Zn^{2+}

Since the prerequisite for detection is a solid-phase extraction process, during which the sensor molecules bind the dissolved Zn^{2+} from the sample, the extraction ability was investigated prior to the fluorescence response. This study was carried out by using single-component, homogeneous samples in the concentration range of 15–3000 ppb Zn^{2+} . The extracted amount of Zn^{2+} was determined after applying the general measurement protocol and the subsequent regeneration process (Section 3.2). Studies revealed that almost the total amount of dissolved Zn^{2+} (>95% in each case) was reversibly complexed by the immobilized sensor molecules during the solid-phase extraction process. The observed high extraction ability was supported by the optimization: sensor molecules were present in excess to the Zn^{2+} content in the entire concentration range of the quantitation. According to the results, the extraction ability of the MNPs does not hinder optochemical analysis in the linear working range of concentration. In the cases of analyzing highly heterogeneous samples, the extraction ability is expected to decrease.

Initially, titration was carried out by using single-component, aqueous solutions of Zn^{2+} of a wide concentration range. The obtained series of spectra can be seen in Figure 4.

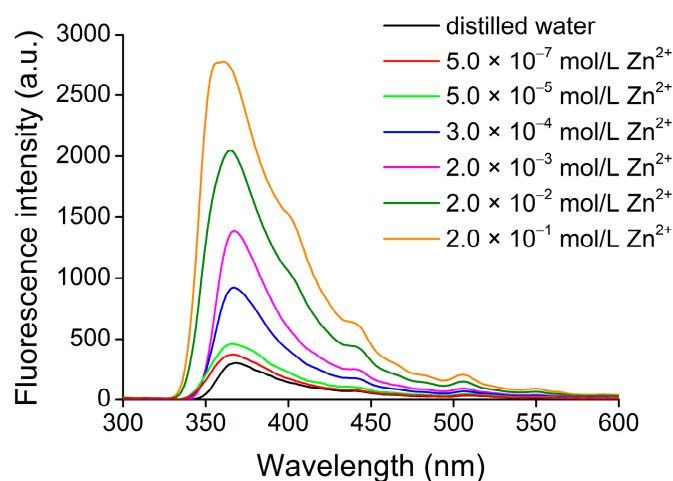


Figure 4. Series of spectra for fluorescence titration of the functionalized MNPs, using single-component aqueous solutions of Zn^{2+} ($\lambda_{\text{excitation}} = 250 \text{ nm}$).

The emission peak wavelength was 370 nm and an 8.7-fold fluorescence enhancement was observed in the 1.0×10^{-8} – 2.0×10^{-1} mol/L Zn^{2+} concentration range while applying excitation at 250 nm. It is important to mention that not all of the immobilized sensor molecules serve as active binding sites for Zn^{2+} due to the presence of numerous adverse effects on ion-trap conformation.

Figure 5 shows the titration curve reported at the emission peak maximum of 370 nm.

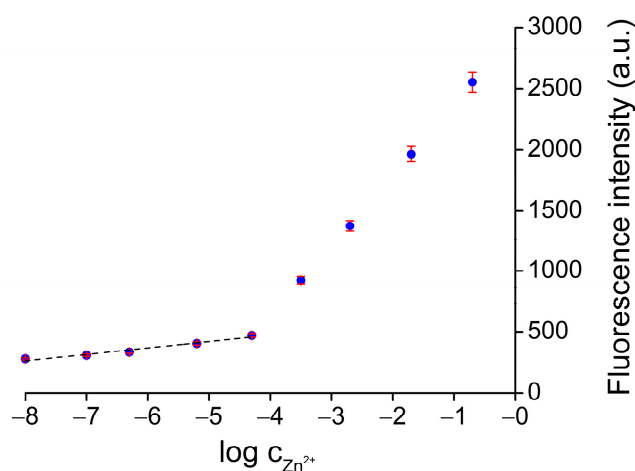


Figure 5. Changes in the fluorescence intensities of the titration spectra at 370 nm as a function of the logarithm of the Zn^{2+} concentration.

The relative standard deviation was within 3.2%. A linear dynamic range of optical response was obtained below 3000 ppb ($F = 52.3 \cdot \log c_{\text{Zn}^{2+}} + 682.8$; $R^2 = 0.97$). The LOD was calculated as 5 ppb, while the LOQ was determined to be 15 ppb. The linearity is also reliable ($R^2 = 0.99$) at higher concentration levels, with an altered slope of the calibration curve. However, quantitation was optimized for concentrations below 3000 ppb. For determining higher Zn^{2+} concentrations, the relative quantity of the MNPs needs to be increased, attributed to the limited binding capacity of the immobilized fluoroionophores.

It is noteworthy to mention that an incubation time is required to reach the equilibrium of complex formation to obtain a constant response. It usually takes more time in the case of immobilized ionophores compared to dissolved ones. Studies were carried out to determine the smallest sufficient time of magnetic stirring before fluorescent determination (Figure 6).

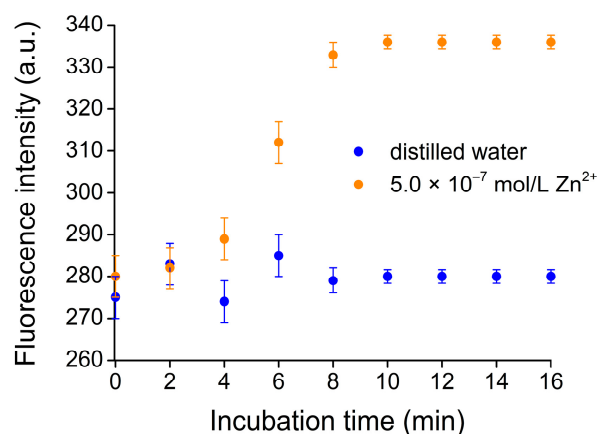


Figure 6. Time dependence of fluorescence response in the presence and absence of Zn^{2+} ($\lambda_{excitation} = 250$ nm, $\lambda_{detection} = 370$ nm).

In the case of the studied samples, a 10 min incubation proved to be enough to achieve a constant signal with a lower deviation. However, depending on the heterogeneity of the samples, more time might be needed.

3.4. Study on Reversibility and Reusability

To obtain insight into the regenerability of the proposed sensing nanoparticles, single-component aqueous samples of the same Zn^{2+} concentration (5.0×10^{-7} mol/L) were measured five times while reporting the observed optical response (Figure 7). Between every repeated measurement, the earlier-mentioned slightly acidic treatment (see Section 3.2) was applied for regeneration.

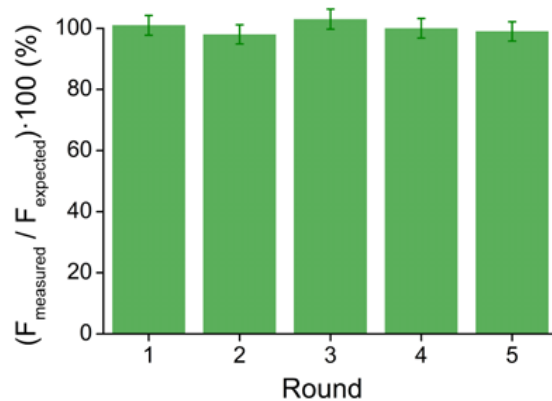


Figure 7. Studies on reusability through the repeated determination of 5.0×10^{-7} mol/L Zn^{2+} samples ($F_{measured}$ refers to the measured fluorescence intensity at 370 nm, while $F_{expected}$ corresponds to the calibration curve at the same wavelength).

The results show that only marginal changes of less than 3.0% were observed between the induced changes in fluorescence, which can be attributed to the effective covalent immobilization and highly reversible complexation of the sensor molecules.

3.5. Study on Selectivity

Studies were also carried out on selectivity to prove that immobilization had no effect on the complexation behavior of the fluoroionophore (1). The fluorescence change was investigated in the equimolar presence of the previously mentioned metal salts (see Section 2.1) upon excitation at 250 nm (Figure 8A), and after that, also under competitive conditions in the simultaneous presence of all indifferent ions (Figure 8B).

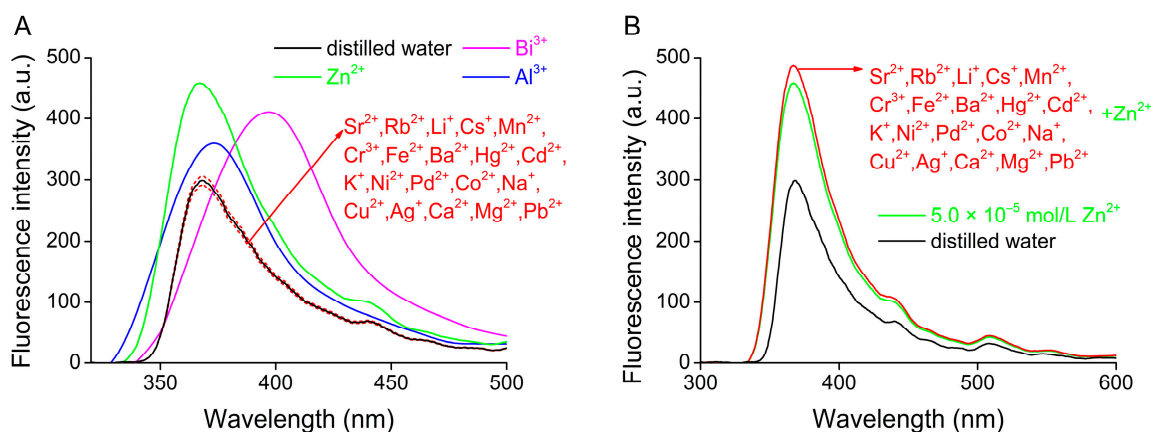


Figure 8. Studies on selectivity through separate measurements of 5.0×10^{-5} mol/L aqueous samples of potentially competing metal ions (A) and those under competitive conditions in the presence of 1.0×10^{-3} mol/L background electrolytes as a mixture of the 20 indifferent ions with 5.0×10^{-5} mol/L individual concentrations, while adding 5.0×10^{-5} mol/L of Zn^{2+} (B) ($\lambda_{\text{excitation}} = 250$ nm).

It can clearly be seen that no significant change (within 5.0%) was caused in the fluorescence by the majority of the metal ions, except Al^{3+} and Bi^{3+} . This interference was expected from the preliminary studies on the free ionophore [35]. However, these competing ions are rarely co-present with Zn^{2+} in real samples; thus, this competition does not hinder practical applicability. We found that the equimolar copresence of the 20 metal ions, which proved to be indifferent, also did not influence the response toward Zn^{2+} significantly. The deviance compared to the single-component Zn^{2+} sample was only within 6%. This observation also indicates that the sensor molecules strongly coordinate Zn^{2+} , even in the presence of Cd^{2+} , Pb^{2+} , Hg^{2+} , Co^{2+} , Ni^{2+} , and Cu^{2+} , which are considered typical competitors in similar chemosensing applications [8].

The obtained selectivity was compared with that of the dissolved ionophore [35] to reveal the effects of nanocores and immobilization on both molecular recognition and signaling. Based on the comparison, both the complexing and signaling properties of the sensor molecule could quite effectively be preserved despite the covalent immobilization. The presence of Zn^{2+} still caused the largest fluorescence enhancement without significant shifts in the emission peak wavelength, while the addition of Al^{3+} and Bi^{3+} additionally caused a slight bathochromic shift. None of the other studied ions showed significant interference with the preferred ones. All of these observations are the same for the dissolved and immobilized sensor molecules. The enhancement of the fluorescence upon the complexation of the preferred ions was smaller compared to the case of the dissolved ionophores. It can be attributed to the fact that not all of the immobilized ionophores can be considered active for complexation, and the optical effects of the non-fluorogenic nanocores can also reduce the sensitivity of detection.

An exact explanation of selectivity cannot be given based on the similarities of the ionic radii or the electronic configuration of the complexed cations. There are several reported optochemical ionophores containing the same 4,5-dimethylacridine fluorophore unit, such as our proposed sensor molecule. These structurally analogue sensor molecules typically show selectivity for soft electrophilic cations like Hg^{2+} [37], Cd^{2+} [37–40], Zn^{2+} [39], Ni^{2+} [41], and Fe^{3+} [41,42]. This is attributed to their soft nucleophilic acridine-*N* and two—usually tertiary—aliphatic *N*-atoms, which have lone electron pairs for coordination. Thus, the observed selectivity is not surprising. After making an overview on recently published Al^{3+} - and Bi^{3+} -selective sensor molecules, it can be seen that almost every coordination sphere consists of a tertiary aliphatic *N* with a lone electron pair and additionally coordinating *O*-centers within a 2–4-atom distance [43–48]. Among the studied competing ions, the trivalent cations, i.e., Cr^{3+} , interfere in general [47,48]. It is also important to

mention that only one example could be found when selectivity toward Bi^{3+} and Al^{3+} were investigated together, and this study also reported the competition of these two cations [43].

3.6. Study on pH Dependence

The pH values of the samples were varied by adding corresponding amounts of aqueous solutions of nitric acid or sodium hydroxide to the aqueous colloid samples of the MNPs containing 5.0×10^{-7} mol/L of Zn^{2+} . The results can be seen in Figure 9.

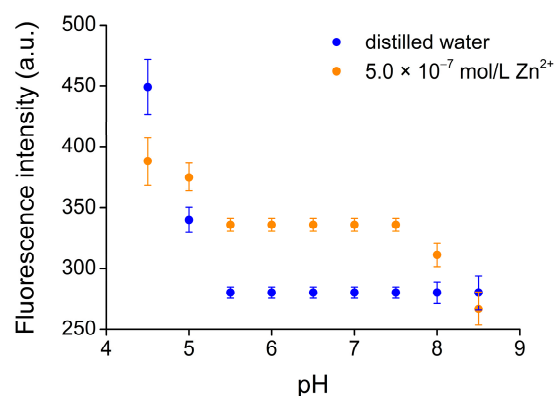


Figure 9. The pH dependence of the fluorescent response toward 5.0×10^{-7} mol/L of Zn^{2+} at 370 nm ($\lambda_{excitation} = 250$ nm).

In the pH interval of 5.5 to 7.5, a constant signal was obtained, indicating a pH-independent working range, which covers the most relevant pH range of the environmental and biological samples. Below pH = 5.5, the basic nitrogens of the sensor molecule can accept protons, which causes a reduced stability of the Zn^{2+} complex, which can be exploited effectively for regeneration (see Figure 3). The protonation of the ionophore (1) can also take place in the absence of Zn^{2+} . The pH range above 7.5 is not considered relevant due to the expected precipitation of the dissolved Zn^{2+} .

3.7. Validation by Analyzing Real Samples

Untreated river water and an aqueous suspension of pumpkin seed flour were measured as heterogeneous multicomponent samples with a natural Zn^{2+} content. Detailed information regarding these samples can be found in the Supplementary Materials. The results were compared with those measured via ICP-OES (Table 1).

Table 1. Application of the fluorescence probe for determining the Zn^{2+} content of untreated river water and an aqueous suspension of pumpkin seed flour.

	River Water	Aqueous Suspension of Pumpkin Seed Flour
Real $c_{\text{Zn}^{2+}}$ ¹	50 ppb	105 ppb
$F_{theoretical}$ ²	358	375
$\bar{F}_{observed}$	344	352
Determined $c_{\text{Zn}^{2+}}$ ³	27 ± 8 ppb	39 ± 11 ppb

¹ The real concentration of Zn^{2+} measured via ICP-OES. ² The theoretically expected fluorescence intensity for Zn^{2+} based on its concentration measured via ICP-OES. ³ The concentration of Zn^{2+} calculated according to the reported equation of the linear regression on the calibration curve (Section 3.3).

Real $c_{\text{Zn}^{2+}}$ $F_{theoretical}$ $\bar{F}_{observed}$ Determined $c_{\text{Zn}^{2+}}$ Meeting our expectations, both the accuracy and precision are inferior to those of the ICP-OES method. The results show that lower concentrations were determined using the proposed probe than the real concentration of Zn^{2+} in all cases. This can be attributed to the fact that not all the Zn^{2+} contents can be complexed with the fluoroionophore, and partial decomplexation can also take place

during the magnetic-assisted solid-phase extraction of the MNPs. Moreover, in the cases of highly contaminated heterogeneous samples, the extraction ability of the particles is expected to decrease due to the nonspecific adsorption of the physical contaminants and the hindered complexation of the sensor molecules. The measurements also revealed that only about 10% of the total Zn^{2+} content of the pumpkin seed flour is dissolved in the sample (the remaining amount is inside the solid part of the sample). Naturally, the proposed probe is only suitable for giving a rough estimation for the dissolved form of Zn^{2+} without any prior treatment of the sample.

4. Evaluation of the Results through Comparisons with Other Methods

The most recent and relevant reported works on the NP-based selective fluorescent optosensing of Zn^{2+} were collected to put the obtained results into context and support the evaluation of the properties of the proposed probe (Table 2).

Table 2. Main operating characteristics of the recently reported, most relevant NP-based fluorescent probes for Zn^{2+} .

NP Type	Magnetic Property (✓ or ✗) ¹	LOD (ppb)	Linear Range of Optical Response (ppb)	Reference
Fe ₃ O ₄ nanomagnet functionalized with dopamine-naphthalimide-dipicolylamine	✓	3.5×10^{-2}	0–1308	[8]
N-(2-(bis(pyridine-2-ylmethyl)amino)ethyl)-2-mercaptoacetamide modified gold NP	✗	1.8×10^{-5}	65–7848	[30]
BODIPY-based self-assembled NPs	✗	4	65–654	[31]
Water-soluble Ag ₂ S quantum dots	✗	50	50–2616	[32]
4-Amino-2-methyl-8-(trifluoromethyl)quinoline functionalized silica-coated Fe ₃ O ₄ nanomagnet	✓	0.4	not reported	[33]
DNAzyme-modified magnetic microbeads	✓	2.2×10^{-6}	6.5×10^{-6} –0.72	[34]
8-Amimoquinoline(N-(quinolin-8-yl)-2-(3-(triethoxysilyl)propylamino)acetamide) functionalized silica-coated Fe ₃ O ₄ nanomagnet	✓	not reported	not reported	[49]
Carbon dots from glucose combined with non-bounded fluorogenic quercetin	✗	131	131–6540	[50]
Magnetic functionalized terbium coordination polymer-adsorbent	✓	14	14–10,464	[51]
Commercially available silica-coated TurboBeads™ functionalized with fluorogenic crown ether	✓	5	15–3000	present work

¹ Refers to the nature of the core of the NP, whether it is magnetic (✓) or not (✗).

A comparison with data from the literature supports the competitiveness of the developed method. Although the obtained LOD is three orders of magnitude lower than the WHO acceptance limit for drinking water, it cannot be considered outstanding among the other alternatives. It can be concluded that each reported method has its own advantages; thus, users are responsible for choosing the most suitable one for the target tasks, for example, based on the linear dynamic ranges. It is also important to note that those methods, which reported the functionalization of typically single-use, non-magnetic nanocores (indicated with '✗' in Table 2) are not able to analyze strongly contaminated samples, especially heterogeneous ones, such as suspensions. Furthermore, they themselves can cause sample contamination, while in the absence of magnetic solid-phase extraction,

the presence of the various background materials can strongly influence the optical response. In general, the introduction of supramolecular host molecules, instead of exploiting simpler functional group-driven coordination, contributes to reducing non-specific adsorption. This was shown in the present case as well, since the applied probe showed less influence (i.e., a weaker fluorescence response) from possible competing agents like Cd^{2+} or other metal ions compared to the majority of the reported alternatives [8,31–34,50,51]. Also, many other methods use chelating additives, like EDTA, for regeneration [8,33]. Comparisons with less advanced Zn^{2+} -selective fluorescent probes (e.g., the application of dissolved ionophores, single-use materials and tests, optode membranes regardless of the type of ionophore immobilization, etc.) are not discussed here. They need a more extended preliminary preparation of samples, despite the fact that their applicability covers a narrower range of analytical challenges.

5. Conclusions

The basic concept of our work involves overcoming the limitations of Zn^{2+} -selective ionophore-based fluorescent analyses in suspensions, which is considered one of the most unfavorable conditions for optical chemosensing. We present here a simple alternative for the covalent modification of a commercially available MNP core, which can also serve as a starting point for future development by applying other ionophores. Qualitative analyses were successfully performed, but the probe was only suitable for giving a rough quantitative estimation for Zn^{2+} content. Applicability was clearly demonstrated, even in real heterogeneous multicomponent samples, while comparison studies revealed a competitive performance to previous results in the literature. The main advantages of the present method are the lack of interference from Cd^{2+} and any relevant anions, the fast and simple regeneration, no sample preparation in general, and the direct applicability for heterogeneous samples. In addition, there is no obstacle to expanding the application in the future of the proposed probe for the rarely investigated Bi^{3+} or for bioimaging in living cells.

Supplementary Materials: The following supporting information can be downloaded at <https://www.mdpi.com/article/10.3390/chemosensors11100547/s1>: Table S1: Metal ion composition of the investigated river water samples determined by ICP-OES; Table S2: Composition of the investigated pumpkin seed flour calculated for 100 g; Figure S1: Concentration-dependent absorption of fluoroionophore 1 in chloroform; Figure S2: UV-absorbance-based calibration curve of fluoroionophore 1 at 250 nm used for calculating its concentration ($R^2 = 0.99$); Figure S3: Linear regression for the optochemical responses in the presence of low concentrations of Zn^{2+} .

Author Contributions: Conceptualization, Á.G.; methodology, Á.G.; formal analysis, P.V.; investigation, P.V. and Á.G.; resources, P.H.; writing—original draft preparation, P.V. and Á.G.; writing—review and editing, T.T. and P.H.; visualization, P.V.; project administration, Á.G.; funding acquisition, P.H. All authors have read and agreed to the published version of the manuscript.

Funding: This research was funded by the National Research, Development, and Innovation Office (grant number K128473), supported by the ÚNKP-23-4-II-BME-127 New National Excellence Program of the Ministry for Culture and Innovation from the source of the National Research, Development, and Innovation Fund.



Data Availability Statement: The authors confirm that the data supporting the findings of this study are available within the article and its Supplementary Materials.

Acknowledgments: The authors express their thanks to Dániel Ster for his valuable technical assistance during this work. Special thanks to the Photonics Department of the Centre for Energy Research for their help and assistance, especially to Dániel Zámbo for his helpful suggestions on this work.

Thanks to László Bezúr for the multielement sample analyses. Thanks to Dennis Mitchell for revising the English language and style.

Conflicts of Interest: The authors declare no conflict of interest. The funding institution had no role in the design of the study; in the collection, analyses, or interpretation of data; in the writing of the manuscript; or in the decision to publish the results.

References

1. Sarkar, K.; Dhara, K.; Nandi, M.; Roy, P.; Bhaumik, A.; Banerjee, P. Selective zinc(II)-ion fluorescence sensing by a functionalized mesoporous material covalently grafted with a fluorescent chromophore and consequent biological applications. *Adv. Funct. Mater.* **2009**, *19*, 223–234. [CrossRef]
2. Dong, Z.; Dong, Z.; Wang, P.; Tian, X.; Geng, H.; Li, R.; Ma, J. A fluorescent probe for zinc detection based on organically functionalized SBA-15. *Appl. Surf. Sci.* **2010**, *257*, 802–806. [CrossRef]
3. Golcs, Á.; Kovács, K.; Vezse, P.; Bezúr, L.; Huszthy, P.; Tóth, T. A cuvette-compatible Zn²⁺ sensing tool for conventional spectrofluorometers prepared by copolymerization of macrocyclic fluoroionophores on quartz glass surface. *Methods Appl. Fluoresc.* **2022**, *10*, 035005. [CrossRef]
4. Pratiwi, F.W.; Kuo, C.W.; Chen, B.C.; Chen, P. Recent advances in the use of fluorescent nanoparticles for bioimaging. *Nanomedicine* **2019**, *14*, 1759–1769. [CrossRef] [PubMed]
5. Chasapis, C.T.; Ntoupa, P.S.A.; Spiliopoulou, C.A.; Stefanidou, M.E. Recent aspects of the effects of zinc on human health. *Arch. Toxicol.* **2020**, *94*, 1443–1460. [CrossRef] [PubMed]
6. Paderni, D.; Giorgi, L.; Voccia, M.; Formica, M.; Caporaso, L.; Macedi, E.; Fusi, V. A new benzoxazole-based fluorescent macrocyclic chemosensor for optical detection of Zn²⁺ and Cd²⁺. *Chemosensors* **2022**, *10*, 188. [CrossRef]
7. Suh, B.; Gil, D.; Yoon, S.; Kim, K.T.; Kim, C. A practical hydrazine-carbothioamide-based fluorescent probe for the detection of Zn²⁺: Applications to paper strip, zebrafish and water samples. *Chemosensors* **2022**, *10*, 32. [CrossRef]
8. Kim, K.T.; Yoon, S.A.; Ahn, J.; Choi, Y.; Lee, M.H.; Jung, J.H.; Park, J. Synthesis of fluorescent naphthalimide-functionalized Fe₃O₄ nanoparticles and their application for the selective detection of Zn²⁺ present in contaminated soil. *Sens. Actuators B Chem.* **2017**, *243*, 1034–1041. [CrossRef]
9. World Health Organization. *Zinc in Drinking-Water. Background Document for Preparation of WHO Guidelines for Drinking-Water Quality*; World Health Organization: Geneva, Switzerland, 2003; Document No.: WHO/SDE/WSH/03.04/17. Available online: https://cdn.who.int/media/docs/default-source/wash-documents/wash-chemicals/zinc.pdf?sfvrsn=9529d066_4 (accessed on 18 September 2022).
10. Shiller, A.M.; Boyle, E. Dissolved zinc in rivers. *Nature* **1985**, *317*, 49–52. [CrossRef]
11. Zhang, S.; Han, G.; Gao, X. The urbanization impacts on potentially toxic metals: The distribution, sources and contamination risks in river situated in typical megacity, China. *Sustain. Cities Soc.* **2023**, *97*, 104784. [CrossRef]
12. Sun, X.; Rosa-Gastaldo, D.; De Biasi, F.; Rastrelli, F.; Mancin, F. ¹H NMR chemosensing of potassium ions enabled by guest-induced selectivity switch of a gold nanoparticle/crown ether nanoreceptor. *ChemPlusChem* **2019**, *84*, 1498–1502. [CrossRef]
13. Deymehkar, E.; Taher, M.A.; Karami, C.; Arman, A. Synthesis of SPR nanosensor using gold nanoparticles and its application to copper(II) determination. *Silicon* **2018**, *10*, 1329–1336. [CrossRef]
14. Kakhki, R.M.; Rakhshanipour, M. Application of nanoparticle modified with crown ether in colorimetric determinations. *Arab. J. Chem.* **2019**, *12*, 3096–3107. [CrossRef]
15. Wang, C.; Sun, F.; He, G.; Zhao, H.; Tian, L.; Cheng, Y.; Li, G. Noble metal nanoparticles meet molecular cages: A tale of integration and synergy. *Curr. Opin. Colloid Interface Sci.* **2022**, *63*, 101660. [CrossRef]
16. Salvia, M.V.; Salassa, G.; Rastrelli, F.; Mancin, F. Turning supramolecular receptors into chemosensors by nanoparticle-assisted “NMR chemosensing”. *J. Am. Chem. Soc.* **2015**, *137*, 11399–11406. [CrossRef] [PubMed]
17. Müller, B.J.; Zhdanov, A.V.; Borisov, S.M.; Foley, T.; Okkelman, I.A.; Tsytsarev, V.; Tang, Q.; Erzurumlu, R.S.; Chen, Y.; Zhang, H.; et al. Nanoparticle-based fluoroionophore for analysis of potassium ion dynamics in 3D tissue models and in vivo. *Adv. Funct. Mater.* **2018**, *28*, 1704598. [CrossRef] [PubMed]
18. Bakker, E.; Bühlmann, P.; Pretsch, E. Carrier-based ion-selective electrodes and bulk optodes. 1. General characteristics. *Chem. Rev.* **1997**, *97*, 3083–3132. [CrossRef]
19. Geißler, D.; Nirmalanathan-Budau, N.; Scholtz, L.; Tavernaro, I.; Resch-Genger, U. Analyzing the surface of functional nanomaterials—How to quantify the total and derivatizable number of functional groups and ligands. *Mikrochim. Acta* **2021**, *188*, 321. [CrossRef] [PubMed]
20. Lakatos, S.; Fetter, J.; Bertha, F.; Huszthy, P.; Tóth, T.; Farkas, V.; Orosz, G.; Hollósi, M. Preparation of a new chiral acridino-18-crown-6 ether-based stationary phase for enantioseparation of racemic protonated primary aralkyl amines. *Tetrahedron* **2008**, *64*, 1012–1022. [CrossRef]
21. Kobayashi, Y.; Gu, S.; Nagao, D.; Konno, M. Direct coating of particles by a liquid phase process. *Curr. Nanosci.* **2007**, *3*, 222–240. [CrossRef]
22. Kumar, S.; Ten Siethoff, L.; Persson, M.; Albet-Torres, N.; Månsson, A. Magnetic capture from blood rescues molecular motor function in diagnostic nanodevices. *J. Nanobiotechnol.* **2013**, *11*, 14. [CrossRef] [PubMed]

23. Zlateski, V.; Fuhrer, R.; Koehler, F.M.; Wharry, S.; Zeltner, M.; Stark, W.J.; Moody, T.S.; Grass, R.N. Efficient magnetic recycling of covalently attached enzymes on carbon-coated metallic nanomagnets. *Bioconjug. Chem.* **2014**, *25*, 677–684. [[CrossRef](#)] [[PubMed](#)]
24. Herrmann, I.K.; Schlegel, A.; Graf, R.; Schumacher, C.M.; Senn, N.; Hasler, M.; Gschwind, S.; Hirt, A.-M.; Günther, D.; Clavien, P.-A.; et al. Nanomagnet-based removal of lead and digoxin from living rats. *Nanoscale* **2013**, *5*, 8718–8723. [[CrossRef](#)] [[PubMed](#)]
25. Sá, J.; Szlachetko, J.; Sikora, M.; Kavčič, M.; Safonova, O.V.; Nachttegaal, M. Magnetic manipulation of molecules on a non-magnetic catalytic surface. *Nanoscale* **2013**, *5*, 8462–8465. [[CrossRef](#)] [[PubMed](#)]
26. Kainz, Q.M.; Zeltner, M.; Rossier, M.; Stark, W.J.; Reiser, O. Synthesis of trisubstituted ureas by a multistep sequence utilizing recyclable magnetic reagents and scavengers. *Chem. Eur. J.* **2013**, *19*, 10038–10045. [[CrossRef](#)] [[PubMed](#)]
27. Kawasaki, H.; Nakai, K.; Arakawa, R.; Athanassiou, E.K.; Grass, R.N.; Stark, W.J. Functionalized graphene-coated cobalt nanoparticles for highly efficient surface-assisted laser desorption/ionization mass spectrometry analysis. *Anal. Chem.* **2012**, *84*, 9268–9275. [[CrossRef](#)] [[PubMed](#)]
28. Wang, F.; Wang, K.; Kong, Q.; Wang, J.; Xi, D.; Gu, B.; Lu, S.; Wei, T.; Chen, X. Recent studies focusing on the development of fluorescence probes for zinc ion. *Coord. Chem. Rev.* **2021**, *429*, 213636. [[CrossRef](#)]
29. Sadananda, D.; Mallikarjunaswamy, A.M.M.; Prashantha, C.N.; Mala, R.; Gouthami, K.; Lakshminarayana, L.; Ferreira, L.F.R.; Bilal, M.; Rahdar, A.; Mulla, S.I. Recent development in chemosensor probes for the detection and imaging of zinc ions: A systematic review. *Chem. Pap.* **2022**, *76*, 5997–6015. [[CrossRef](#)]
30. Li, D.; Ma, Y.; Duan, H.; Jiang, F.; Deng, W.; Ren, X. Fluorescent/SERS dual-sensing and imaging of intracellular Zn²⁺. *Anal. Chim. Acta* **2018**, *1038*, 148–156. [[CrossRef](#)]
31. Jia, M.Y.; Wang, Y.; Liu, Y.; Niu, L.Y.; Feng, L. BODIPY-based self-assembled nanoparticles as fluorescence turn-on sensor for the selective detection of zinc in human hair. *Biosens. Bioelectron.* **2016**, *85*, 515–521. [[CrossRef](#)]
32. Wu, Q.; Zhou, M.; Shi, J.; Li, Q.; Yang, M.; Zhang, Z. Synthesis of water-soluble Ag₂S quantum dots with fluorescence in the second near-infrared window for turn-on detection of Zn(II) and Cd(II). *Anal. Chem.* **2017**, *89*, 6616–6623. [[CrossRef](#)]
33. Pourfallah, G.; Lou, X. Novel 4-amino-2-methyl-8-(trifluoromethyl)quinoline-based magnetic nanostructures for highly sensitive detection of zinc ions in aqueous solutions. *Dyes Pigm.* **2018**, *158*, 12–19. [[CrossRef](#)]
34. Shen, W.; Li, Y.; Qi, T.; Wang, S.; Sun, J.; Deng, H.; Lu, H.; Chen, C.; Chen, L.; Tang, S. Fluorometric determination of zinc(II) by using DNAzyme-modified magnetic microbeads. *Microchim. Acta* **2018**, *185*, 447. [[CrossRef](#)]
35. Golcs, Á.; Kovács, K.; Vezse, P.; Tóth, T.; Huszthy, P. Acridino-diaza-20-crown-6 ethers: New macrocyclic hosts for optochemical metal ion sensing. *Molecules* **2021**, *26*, 4043. [[CrossRef](#)] [[PubMed](#)]
36. Long, G.L.; Winefordner, J.D. Limit of detection. A closer look at the IUPAC definition. *Anal. Chem.* **1983**, *55*, 712A–724A.
37. Lee, H.N.; Kim, H.N.; Swamy, K.M.K.; Park, M.S.; Kim, J.; Lee, H.; Park, S.; Yoon, J. New acridine derivatives bearing immobilized azacrown or azathiacrown ligand as fluorescent chemosensors for Hg²⁺ and Cd²⁺. *Tetrahedron Lett.* **2008**, *49*, 1261–1265. [[CrossRef](#)]
38. dos Santos Carlos, F.; da Silva, L.A.; Zanlorenzi, C.; Nunes, F.S. A novel macrocycle acridine-based fluorescent chemosensor for selective detection of Cd²⁺ in Brazilian sugarcane spirit and tobacco cigarette smoke extract. *Inorg. Chim. Acta* **2020**, *508*, 119634–119641. [[CrossRef](#)]
39. Visscher, A.; Bachmann, S.; Schnegelsberg, C.; Teuteberg, T.; Mata, R.A.; Stalke, D. Highly selective and sensitive fluorescence detection of Zn²⁺ and Cd²⁺ ions by using an acridine sensor. *Dalton Trans.* **2016**, *45*, 5689–5699. [[CrossRef](#)] [[PubMed](#)]
40. Wang, Y.; Hu, X.; Wang, L.; Shang, Z.; Chao, J.; Jin, W. A new acridine derivative as a highly selective ‘off-on’ fluorescence chemosensor for Cd²⁺ in aqueous media. *Sens. Actuators B Chem.* **2011**, *156*, 126–131. [[CrossRef](#)]
41. Wang, C.; Fu, J.; Yao, K.; Xue, K.; Xu, K.; Pang, X. Acridine-based fluorescence chemosensors for selective sensing of Fe³⁺ and Ni²⁺ ions. *Spectrochim. Acta A* **2018**, *199*, 403–411. [[CrossRef](#)] [[PubMed](#)]
42. Zhou, J.; Yuan, Y.F.; Zhuo, J.B.; Lin, C.X. Synthesis and characterization of cyclophane: The highly selective recognition of Fe³⁺ in aqueous solution and H₂PO₄[−] in acetonitrile solution. *Tetrahedron Lett.* **2018**, *59*, 1059–1064. [[CrossRef](#)]
43. Saravanan, A.; Shyamsivappan, S.; Suresh, T.; Subashini, G.; Kadirvelu, K.; Bhuvanesh, N.; Nandhakumar, R.; Mohan, P.S. An efficient new dual fluorescent pyrene based chemosensor for the detection of bismuth(III) and aluminium(III) ions and its applications in bio-imaging. *Talanta* **2019**, *198*, 249–256. [[CrossRef](#)] [[PubMed](#)]
44. El-Sewify, I.M.; Shenashen, M.A.; Shahat, A.; Yamaguchi, H.; Selim, M.M.; Khalil, M.M.; El-Safty, S.A. Dual colorimetric and fluorometric monitoring of Bi³⁺ ions in water using supermicroporous Zr-MOFs chemosensors. *J. Lumin.* **2018**, *198*, 438–448. [[CrossRef](#)]
45. Ramasamy, K.; Thambusamy, S. Dual emission and pH based naphthalimide derivative fluorescent sensor for the detection of Bi³⁺. *Sens. Actuators B Chem.* **2017**, *247*, 632–640. [[CrossRef](#)]
46. Zhang, E.; Ju, P.; Li, Q.; Hou, X.; Yang, H.; Yang, X.; Zou, Y.; Zhang, Y. A novel rhodamine 6G-based fluorescent and colorimetric probe for Bi³⁺: Synthesis, selectivity, sensitivity and potential applications. *Sens. Actuators B Chem.* **2018**, *260*, 204–212. [[CrossRef](#)]
47. Yue, X.L.; Wang, Z.Q.; Li, C.R.; Yang, Z.Y. Naphthalene-derived Al³⁺-selective fluorescent chemosensor based on PET and ESIPT in aqueous solution. *Tetrahedron Lett.* **2017**, *58*, 4532–4537. [[CrossRef](#)]
48. Yu, C.; Jian, L.; Ji, Y.; Zhang, J. Al(III)-responsive “off-on” chemosensor based on rhodamine derivative and its application in cell imaging. *RSC Adv.* **2018**, *8*, 31106–31112. [[CrossRef](#)] [[PubMed](#)]
49. Qiu, L.; Zhou, S.; Li, Y.; Rui, W.; Cui, P.; Zhang, C.; Yu, Y.; Wang, C.; Wang, X.; Wang, J.; et al. Silica-coated Fe₃O₄ nanoparticles as a bifunctional agent for magnetic resonance imaging and ZnII fluorescent sensing. *Technol. Cancer Res. Treat.* **2021**, *20*, 3667–3673. [[CrossRef](#)]

50. Yang, M.; Kong, W.; Li, H.; Liu, J.; Huang, H.; Liu, Y.; Kang, Z. Fluorescent carbon dots for sensitive determination and intracellular imaging of zinc(II) ion. *Microchim. Acta* **2015**, *182*, 2443–2450. [[CrossRef](#)]
51. Xu, S.; Zhang, L.; Zhao, Y.; Luo, Y.; Yu, B.; Zhang, W. A magnetic functionalized lanthanide fluorescent sensor for detection of trace zinc ion. *Res. Chem. Intermed.* **2021**, *47*, 3487–3500. [[CrossRef](#)]

Disclaimer/Publisher’s Note: The statements, opinions and data contained in all publications are solely those of the individual author(s) and contributor(s) and not of MDPI and/or the editor(s). MDPI and/or the editor(s) disclaim responsibility for any injury to people or property resulting from any ideas, methods, instructions or products referred to in the content.